Frustrated tunneling ionization during laser-induced D_2 fragmentation: Detection of excited metastable D^* atoms

J. McKenna, S. Zeng, J. J. Hua, A. M. Sayler, M. Zohrabi, Nora G. Johnson, B. Gaire, K. D. Carnes, B. D. Esry, and I. Ben-Itzhak

J. R. Macdonald Laboratory, Physics Department, Kansas State University, Manhattan, Kansas 66506, USA

(Received 3 August 2011; published 24 October 2011)

In a recent Letter, Manschwetus *et al*. [Phys. Rev. Lett. **102**, 113002 (2009)] reported evidence of electron recapture during strong-field fragmentation of H_2—explained using a frustrated tunneling ionization model. Unusually, the signature of this process was detection of excited H^* atoms. We report here an extensive study of this process in D_2. Our measurements encompass a study of the pulse duration, intensity, ellipticity, and angular distribution dependence of D^* formation. While we find that the mechanism suggested by Manschwetus *et al*. is consistent with our experimental data, our theoretical work shows that electron recollision excitation cannot be completely ruled out as an alternative mechanism for D^* production.

DOI: 10.1103/PhysRevA.84.043425 PACS number(s): 33.80.Rv, 33.80.Wz, 42.50.Hz

I. INTRODUCTION

One of the most important discoveries of intense laser-matter-interaction studies is laser-driven electron recollision. The celebrated three-step model, elucidated by Corkum [1] and Kulander *et al*. [2,3], describes the details of the electron recollision event. In the first step, an intense linearly polarized laser pulse tunnel ionizes an atom or molecule, releasing an electron wave packet to the continuum. The second step involves the subsequent propagation of this electron wave packet in the oscillating electric (E) field of the laser pulse. As the E field periodically reverses direction, the electron wave packet can be driven to and from the core of the parent ion. During the third step, the electron wave packet collides with the parent ion. From this collision a number of phenomena have been observed.

The electron recollision phenomena have been detected in several channels. Elastic scattering is observed in above-threshold ionization photoelectron energy spectra at the high-energy extreme following backscattering of the electron from the parent ion [4]. This scattering process is being harnessed for electron diffraction imaging of atoms [5,6] and molecules [7], with the potential of time-resolved studies of dynamical changes [8]. Inelastic scattering is observed via nonsequential ionization, either by direct electron-impact ionization [9] or through electron-impact excitation followed by field ionization [9,10]. This has been used to resolve attosecond timescale motion of molecular dynamics [11–14]. Electron recombination with the parent ion has been observed by detecting the high-harmonic photons emitted in this process (see, e.g., [15]) or through detection of the particles following the recombination event [16]. Electron recombination is the foundation of the modern era of optical attosecond science [17–19].

Related to electron recombination, Nubbermeyer *et al*. have reported a new mechanism called frustrated tunneling ionization (FTI) [20]. In contrast to traditional electron recombination where an electron makes a near encounter with the ionic core and typically recombines to the atomic ground state, in FTI an electron is recaptured to an excited Rydberg state of the atom. To conserve energy and momentum, this recombination step must take place in the presence of the laser field. Our understanding from the work of Nubbermeyer *et al*. is that the electron is gently decelerated over many laser cycles, gradually transferring its momentum to the field, and is eventually captured into a Rydberg orbital by the Coulomb attraction of the remnant ion core. First observed for He, the signature of FTI is the formation of excited neutral atoms (He^*) that diminish in rate when circularly polarized light is used (suppressing the electron return [1]).

Since the first report of FTI in atoms, Manschwetus *et al*. have observed the formation of excited H^* atoms following strong-field laser fragmentation of H_2 [21] (see also N_2 [22], Ar_2 [23,24], and theory for D_3^+ [25]). In conjunction with these experiments, we have performed measurements of excited D^* atoms from D_2 that we report here. Manschwetus *et al*. concluded that the production scheme of the excited H^* atoms involved the FTI mechanism whereby an ejected electron recombines into an excited Rydberg state of one of the fragments of H_2. The main focus of Ref. [21] was on high-kinetic-energy release (high-KER) H^* fragments (4–9 eV), although H^* fragments with low KER (0–2 eV) were also observed. By a coincidence measurement of H^+ ions with H^* atoms and through comparison with classical trajectory Monte Carlo simulations, the authors determined that the high-kinetic-energy H^* atoms came from Coulomb explosion via $H_2 + n\hbar\omega \rightarrow H^+ + H^+ + 2e^-$, followed by electron recombination of $H^+ + e^- \rightarrow H^*$ (see Fig. 3 of [21])—where $n\hbar\omega$ represents the laser field. Again, from energy and momentum conservation the recombination step should take place on the trailing edge of the laser pulse or while the nuclei are still close enough to interact. It would seem that the former is more feasible from the vision of the FTI process where the electron is gradually decelerated by the laser field.

In this paper we explore this Coulomb explosion process, as well as the production mechanism for the low KER fragments. Using intense 7 and 35 fs, 790 nm laser pulses, we fragment D_2 molecules and measure the resulting excited D^* kinetic energy spectra. From our data we present evidence in support of the frustrated tunneling ionization explanation and compare the D^* spectra with ionic D^+ spectra. We also theoretically consider if electron recollision excitation of D_2^+ could be

used as an alternative mechanism to FTI that could explain the formation of excited atoms. The results show that indeed it cannot be entirely ruled out, although as a whole it does not appear as satisfactory an explanation as FTI. A detailed overview of the dependence of D^* spectra on laser intensity, pulse duration, angular distribution, and ellipticity is presented in the Appendix.

II. EXPERIMENTAL SCHEME

For our measurements we employ an ultrahigh vacuum time-of-flight mass spectrometer setup as illustrated in Fig. 1. Briefly, intense 790 nm Ti:sapphire laser pulses are focused using an $f = 75$ mm spherical mirror onto a gas target of D_2. The direct pulses from our laser system have a transform-limited pulse duration of 35 fs full width at half maximum (FWHM), or can be compressed using a neon-filled hollow-core fiber and chirped mirror arrangement to produce transform-limited 7 fs (FWHM) pulses [26]. The pulses are characterized by frequency-resolved optical gating (FROG) [27]. When focused, the pulses have a peak intensity of up to 2×10^{16} W/cm^2 (35 fs) or 4×10^{16} W/cm^2 (7 fs), while their polarization axis and ellipticity are controlled using half-wave and quarter-wave plates, respectively.

For detection of excited-D^* or D^+ fragments, the time-of-flight mass spectrometer apparatus is operated under different conditions. To detect the D^+ ions, we use Wiley-McLaren space-focusing conditions [28] for the spectrometer fields (with field strengths of 16.3 V/cm and 128 V/cm for the ion extraction and subsequent acceleration regions, respectively) and allow the D^+ ions to then travel field free in the drift region leading to the mesh directly before the microchannel plate (MCP) detector (chevron configuration). An operating voltage of -1800 V, applied to the surface of the front MCP, accelerates the D^+ ions into the MCP for efficient detection.

To detect excited D^* atoms the spectrometer fields are switched off and the breakup momentum of the D^* atoms carries them toward the MCP detector positioned a distance of 0.57 m from the interaction region. A voltage of $+500$ V applied to the mesh in front of the detector repels any positive ions, while the front MCP operating voltage of -1800 V ensures that no electrons are detected. In this way only neutral fragments get through to the detector. We tested several voltage combinations on the spectrometer and detector mesh to block any charged particles, and found that the D^* spectra are insensitive to the exact settings, as expected. We do note, however, that application of a high voltage to the spectrometer could lead to field ionization of D^* Rydberg atoms; thus, for the actual measurements of D^* we keep the spectrometer field switched off.

For both the ion- and atom-detection setups, a small aperture with a solid angle of 2.2×10^{-4} sr, centered on the spectrometer axis, limits the collection angle of the fragments.

The data acquisition system is operated in event-by-event mode by sending the MCP signals through a fast-timing preamplifier, a constant fraction discriminator, and finally recording the signals using a time-to-digital converter. The time-of-flight of the D^+ ions is $\sim$5.3 μs, while the D^* atoms take much longer, in the range of 10–130 μs.

The operation of the MCP to detect slow atoms requires that the atoms are internally excited (see, e.g., [29–31]). The internal energy of the atoms impinging on the MCP releases electrons from the surface of the MCP channels generating a detectable signal. The internal energy must be above the work function of the MCP surface, setting a lower limit on the internal energy of several eV. Since metastable D($2s$) atoms have an internal excitation energy of 10.2 eV, any atom that survives to the detector in this state or above will be efficiently detected. However, the majority of excited states produced will decay to the D($1s$) ground state before reaching the detector and will not be detected. Hence the measured signal level may only represent a fraction of the actual D^* neutrals produced ($\sim$1% [21]).

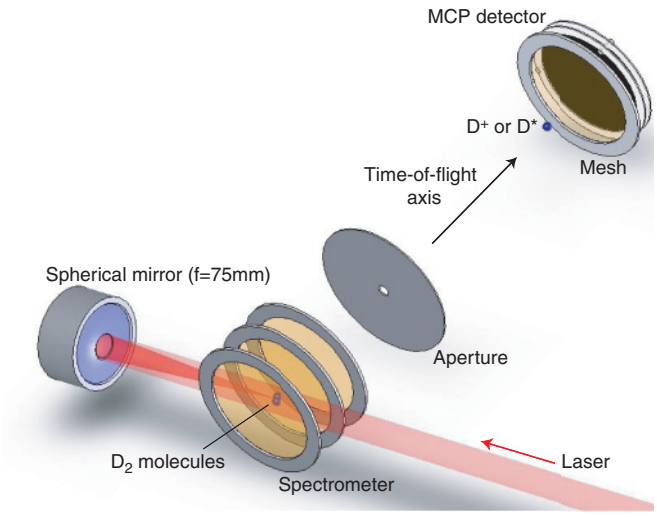

FIG. 1. (Color online) Schematic of time-of-flight mass spectrometer used to image the kinetic energy of D^+ and D^* fragments from D_2 fragmentation by intense 790 nm laser pulses. Diagram is not to scale. See text for details of operation.

III. RESULTS AND DISCUSSION

A. Frustrated tunneling ionization mechanism

We begin by reviewing the work of Manschwetus *et al.* [21]. Figure 2(a) shows a direct comparison of our experiment with the one in Ref. [21] where the KER distribution of excited atom fragments is plotted (arbitrarily normalized to one another). We note that the conditions for the two experiments were quite different and are responsible for the main differences in Fig. 2(a). That is, in Ref. [21] the fragmentation of H_2 using 27 fs, 3×10^{14} W/cm^2 pulses was studied, while here we study D_2 fragmentation using 35 fs, 2×10^{15} W/cm^2 pulses. Nonetheless, the qualitative features are similar and warrant discussion.

In Fig. 2(a), two main features in our D^* data are observed: a low-energy peak centered around 1.2 eV and a high-energy peak centered around 6.5 eV. Both peaks are suppressed using circularly polarized light, as shown in Fig. 2(b) (see also the Appendix). For this linear-circular comparison, the intensities have been matched by keeping the peak E field the same; that is, for circular polarization we use double the input pulse energy as for linear polarization with a peak intensity of 10^{16} W/cm^2.

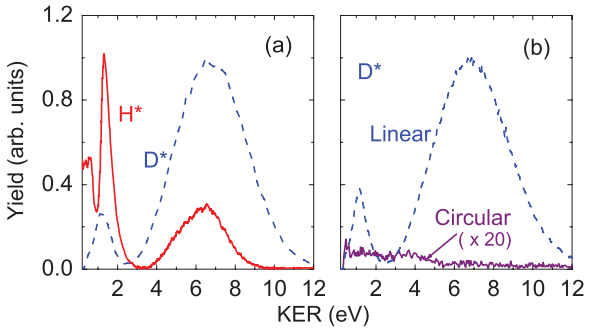

FIG. 2. (Color online) (a) Experimental KER distributions for production of excited H* atoms using 27 fs, 3×10^{14} W/cm^2 pulses (solid curve) reproduced from Manschwetus *et al.* [21], and excited D* atoms using 35 fs, 2×10^{15} W/cm^2 pulses (dashed curve) reported here. (b) D* data (reported here) for linearly (dashed) and circularly (solid) polarized 35 fs pulses (note, circular data are scaled up by a factor of 20 to make visible) at the same peak E field corresponding to an intensity of 10^{16} W/cm^2 for the linear polarization. All spectra are shown for KER > 0.2 eV because, as KER $\rightarrow 0$ eV, the TOF $\rightarrow \infty$ for the atoms.

As discussed in the introduction, Manschwetus *et al.* established that the high-energy peak comes from the laser removal of two electrons from H_2 (D_2) followed by Coulomb explosion of the fragment ions. An electron with insufficient drift energy to escape the vicinity of the fragmenting molecule can be recaptured back by the Coulomb field of one of the H^+ (D^+) ions into a high-lying orbital producing the excited H* (D*) atoms—process "1" in Fig. 3. For the recapture step a third body (photon, proton, or electron) must be present

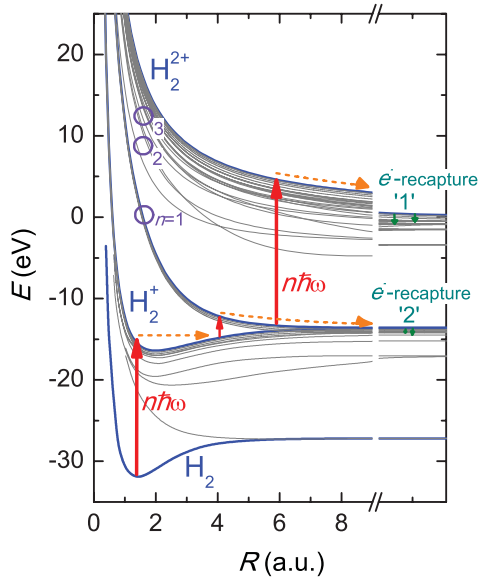

FIG. 3. (Color online) Potential energy curves of the H_2 (D_2) molecule and molecular ions, reproduced from [32,33]. The upward arrows denote laser-induced ionization or excitation, the horizontal arrows denote propagation of the nuclear wave packets, and the small downward arrows denote the electron recapture steps at large R, for high-KER ("1") and low-KER ("2") gain. The circled areas show the points of projection to the excited D_2^+ $n = 1$, $n = 2$, and $n = 3$ states in our calculations— see text.

to conserve energy and momentum. This mechanism was modeled in Ref. [21] using a classical trajectory calculation of the Coulomb exploding H_2^{2+} fragments and the electron (from ionization of H_2^+), and reasonable agreement with the experimental data was found. Furthermore, Manschwetus *et al.* found that the H* peak closely resembles the H^+ Coulomb explosion peak from the $H^+ + H^+$ channel, and that it is absent for circular polarization because this curtails the FTI process [20], as we observe in Fig. 2(b). Based on the similarity of our data with the data presented in Ref. [21], we suspect that the same mechanisms are involved.

The low-energy peak drew less discussion from Manschwetus *et al.* [21]. The authors did, however, note its resemblance to the traditional dissociation peak(s) in H^+ spectra that comes from the reaction $H_2^+ + n\hbar\omega \rightarrow H^+ + H$. This is an important clue to its origin. It would seem that the low-energy peak arises from a mechanism similar to that of the high-energy peak. Namely, after an electron is liberated from H_2 and the subsequent H_2^+ dissociates, the H^+ produced in the reaction recaptures the ionized electron to a highly excited state (H*)—process "2" in Fig. 3. Similar to the high-energy peak, this peak disappears rapidly as the laser polarization is changed from linear to circular [see Fig. 2(b)], suppressing the electron return [1].

The difference in ratio of the low-to-high-energy peaks between the data in Ref. [21] and here [Fig. 2(a)] can be explained by the intensity difference of the experiments. For our experiment the intensity is a factor of ~7 larger than in Ref. [21]. This will increase the amount of Coulomb explosion (high energy) with respect to the dissociation channel (low energy). However, a direct comparison of the two experiments is complicated by different focusing conditions which lead to different focal volume intensity-averaging effects.

B. Classical model of frustrated tunneling ionization

To illustrate how FTI may physically proceed we have modeled it in a similar way to [21] using classical trajectories for the particles (see also [34]). The goal here is not to make a quantitative comparison with our experiments (which would require averaging over many parameters such as laser focal volume intensity, internuclear separation, electron release time, etc.) but rather merely to visualize FTI, as clearly the model is oversimplified.

For the high-KER process we mimic ionization of the transient D_2^+ molecule by separating the D^+ nuclei on a grid along the x coordinate by an internuclear distance of $R =$ 6 a.u. (consistent with charge-resonance enhanced ionization (CREI) [35–37]). The nuclei are then allowed to Coulomb explode near the peak of a 35 fs, 2×10^{15} W/cm^2, 790 nm pulse that is linearly polarized along x. Simultaneously, an electron positioned equidistant between the nuclei is released with a small lateral momentum (0.1 a.u.) in the y direction (i.e., perpendicular to the laser field, see [21,38]). The subsequent motion of the nuclei and electron in the laser field is then monitored as a function of time. For the deuteron-deuteron and deuteron-electron interactions we use softened Coulomb potentials with softening parameters a of 0.03 and 1.0, respectively, as defined in Ref. [39]. Figures 4(a) and 4(b) show the particle trajectories for an example case where the

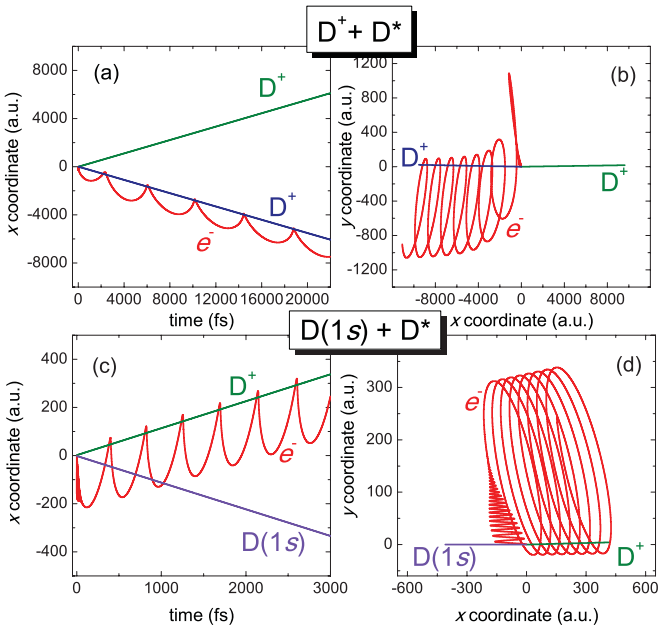

FIG. 4. (Color online) Classical trajectory calculations of FTI leading to the [(a), (b)] $D^+ + D^*$ and [(c), (d)] $D(1s) + D^*$ channels in 35 fs, 2×10^{15} W/cm^2 pulses (see text). Plots (a) and (c) show the x coordinate of the nuclear fragments and electron as a function of time while plots (b) and (d) show an x-y map of the fragment trajectories. The laser is polarized along x. Note that the combination of the electron orbiting a D^+ core in each of the plots leads to the final D^* product.

electron is released 2.4° before the laser field peak (where 360° is one complete laser cycle, i.e., 2.7 fs). The electron initially oscillates in the field of the driving laser pulse (visible only in the figures when zoomed in) but as the field dampens the electron is dragged backward by the Coulomb attraction of a D^+ ion and falls into orbit. Since the screening of the electron is minimal the fragmentation has high KER from the Coulomb explosion event. The end products of the reaction are $D^+ + D^*$—the signature of FTI.

We model low KER similarly but by separating the D^+ and D nuclei by $R = 4.8$ a.u. (equivalent to the one-photon-resonance distance between the $1s\sigma_g$ and $2p\sigma_u$ states of $D_2{}^+$ at 790 nm) and allowing them to interact through the repulsive $D_2{}^+$ $2p\sigma_u$ potential. An example set of trajectories is shown in Figs. 4(c) and 4(d) for an electron released 1.5° before the laser field peak. As before, the electron gradually attaches itself to an excited orbital of D^+ as the laser dies off, thereby forming the products $D(1s) + D^*$.

There are two qualitative outcomes of the classical model of Manschwetus *et al.* [21]. First, it indicates that the electron recapture step is curtailed using circular polarization, as is experimentally observed in Fig. 2(b). While not shown here, we have performed the same calculation as in Fig. 4 but using circularly polarized pulses and find that, for all phases of the electron release, the electron is never recaptured by a D^+ ion. This is because, in a circularly polarized pulse, the electron obtains a large drift momentum in the laser field. This drift momentum, directed away from the nuclei, is too large for the Coulomb attraction of a D^+ ion to overcome, thus FTI never occurs.

Second, from the model one would qualitatively expect that the KER distributions for FTI, namely, the $D^+ + D^*$ and $D(1s) + D^*$ channels, should be similar to the $D^+ + D^+$ and $D(1s) + D^+$channels, respectively. The reason for this is because the electron recapture is a gradual process occurring on the trailing edge of the laser pulse, by which time much of the KER in breakup has already been gained by the nuclei. Even after the electron is effectively captured into a Rydberg orbit its screening of the nuclear charge is minimal because it spends most of its time at a large distance away from the nucleus. Thus, the nuclear dynamics behave the same as when the electron is not captured. A similar phenomenon, namely, partial (or "reduced") screening, has been observed in electron-capture and ionization studies stemming from fast ion-molecule collision experiments [40,41].

C. Consideration of electron recollision excitation

The main experimental evidence that the return of the electrons leads to the formation of D^* fragments is the fact that the D^* contribution diminishes for circular polarization—see Fig. 2(b) and also the Appendix. One is also reminded that our experiment is only sensitive to detection of excited atoms ($\gtrsim$5 eV internal energy); thus, dissociation must be via an excited electronic manifold of D_2 or $D_2{}^+$. We expect that we are primarily measuring fragments in the $D(2s)$ state since all others will have decayed by the time they hit the detector. Any states that do decay to $D(1s)$ will not be detected. Hence what we do measure is likely to represent only a small fraction of the total excited states that were produced in the experiment.

While the FTI mechanism is consistent with both the formation of D^* fragments and their suppression with circular polarization, there is an alternative mechanism that would also fit the bill—involving electron recollision excitation (see, e.g., [11,12]). That is, if a recollision electron inelastically collides with the $D_2{}^+$ core and promotes it to a repulsive excited state, the excited state would dissociate forming $D^+ + D^*$. This mechanism would have a similar suppression as FTI using circularly polarized light because it also involves electron recollision. To check if recollision excitation could explain the experimental observations, we have modeled it by solving the time-dependent Schrödinger equation in the Born-Oppenheimer representation neglecting rotation and allowing only for electronic excitation, but not ionization. Our theoretical method has been described elsewhere [42,43], hence we only outline the specifics of the calculations that apply to this work.

In our model, we assume that D_2 is instantaneously ionized to $D_2{}^+$ at an intensity of 5×10^{13} W/cm^2, where we start the calculation. At this time the D_2 ground-state $v = 0$ wave function is projected onto the $D_2{}^+$ $1s\sigma_g$ state. This projection is equivalent to assuming a coherent Franck-Condon population of the $1s\sigma_g$ vibrational states (although evidence suggests that the population deviates from this distribution depending on the laser parameters [44,45]). The $D_2{}^+$ nuclear wave packet then propagates on the $1s\sigma_g$ state until the removed electron is assumed to return and recollide with the molecule. For our model, we consider only return times that correspond to odd returns since the excitation contribution from even returns is small and may be neglected due to lower electron

recollision energies [13,14]. For 7 fs pulses, it is likely that the first few returns dominate; hence, we consider return times of 1.8 and 4.4 fs, corresponding roughly to the first and third returns, respectively. These are denoted $r_{1.8\ \mathrm{fs}}$ and $r_{4.4\ \mathrm{fs}}$, respectively. For 35 fs pulses, returns when the intensity of the pulse is near its maximum (peak intensity 10^{14} W/cm^2) will dominate since the electron recollision energies are highest. We thus choose return times of 9.7 fs ($r_{9.7\ \mathrm{fs}}$) and 12.3 fs ($r_{12.3\ \mathrm{fs}}$) which classically coincide roughly with the seventh and ninth returns, respectively. At the electron return time, the D_2^+ wave packet is launched onto a higher excited state of D_2^+—see circled areas in Fig. 3. This latter projection simulates the excitation by the recolliding electron, which is a fast process. After this second projection, the wave packet propagates for the remainder of the laser pulse, and we analyze the final kinetic energy release distribution and population on the excited manifold states, i.e., the dissociation limits leading to $D^+ + D(nl)$, where $D(nl)$ is for the $n = 2$, 3, and 4 excited states. We then sum the contributions from these states to give the total dissociation probability on the $D(nl)$ manifolds. Since the molecule is assumed to be aligned to the field, only σ states are included in the calculation (since transitions to π states, from the ground σ state, require perpendicular alignment of the molecule).

For our calculations we used an intensity of 10^{14} W/cm^2. This was the highest that could be used and still avoid any effects of ionization of D_2^+, which are not included in our calculations. We also used pulse durations of 7 and 35 fs to match our experimental data. Figure 5 shows the results of our calculations when we project the D_2^+ wave packet onto the

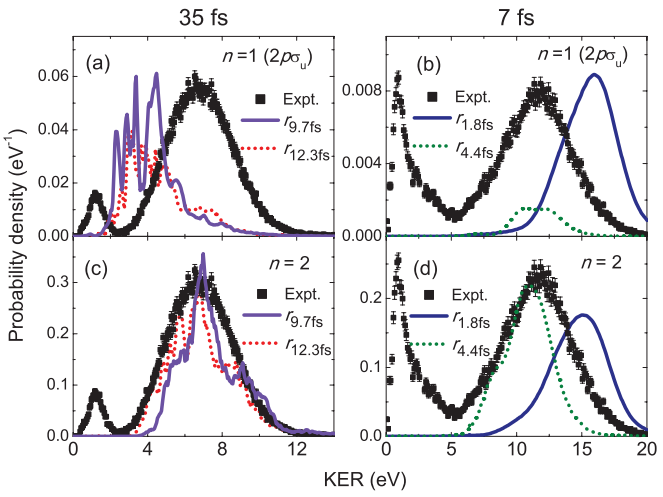

FIG. 5. (Color online) Calculated KER distributions at 10^{14} W/cm^2 from our model of inelastic electron recollision excitation—see text for details. Plots (a) and (b) display results for 35 and 7 fs, respectively, where recollision excitation is to the D_2^+ $n = 1\ 2p\sigma_u$ state, for electron return times of 1.8, 4.4, 9.7, and 12.3 fs, as labeled. The probability is the combination of dissociation to the excited $D^+ + D(nl)$ channels, where $n = 2$, 3, and 4. Plots (c) and (d) are the equivalent for excitation to the $n = 2$ highest σ_g state. For comparison, the data points show the D^* experimental data for 35 fs, 2×10^{15} W/cm^2 and 7 fs, 4×10^{15} W/cm^2 pulses, arbitrarily normalized to the theory. We note the theory and experiment intensities differ (see text for discussion).

$n = 1\ 2p\sigma_u$ state [Figs. 5(a) and 5(b)] and $n = 2$ [Figs. 5(c) and 5(d)] manifold in the electron recollision step. For the $n = 2$ manifold we display only the results for the projection to the highest σ_g state as the other states yield similar KER, as does projection to the $n = 3$ manifold (not shown). For 7 fs, only the $r_{1.8\ \mathrm{fs}}$ and $r_{4.4\ \mathrm{fs}}$ recollision return times are shown, while for 35 fs only the $r_{9.7\ \mathrm{fs}}$ and $r_{12.3\ \mathrm{fs}}$ returns are shown. The data points in the figures are the experimental results at the respective pulse durations—but significantly higher intensity (2×10^{15} W/cm^2 for 35 fs and 4×10^{15}W/cm^2 for 7 fs) than used in the theory. Since the theory does not include intensity averaging over the laser focal volume, however, the effective experiment and theory intensities will actually be more similar. The experimental results will be discussed in further detail in Sec. III D.

Surveying the results, as a whole it would seem that electron recollision excitation cannot be completely ruled out as a potential contributing mechanism to the formation of D^* neutral fragments—although it is by no means entirely satisfactory as an explanation. The evidence to suggest that it could play some role is particularly visible for recollision excitation to the $n = 2$ states [Figs. 5(c) and 5(d)]. For example, at 7 fs, Fig. 5(d) indicates that excitation from recollisions $r_{1.8\ \mathrm{fs}}$ and $r_{4.4\ \mathrm{fs}}$ to the $n = 2$ manifold could conceivably account for the high KER experimental peak centered at around 12 eV. At 35 fs, Fig. 5(c) similarly shows that excitation to the $n = 2$ manifold from later recollision times, $r_{9.7\ \mathrm{fs}}$ and $r_{12.3\ \mathrm{fs}}$ (which coincide with near the peak of the laser pulse), could possibly explain the peak centered at 6.5 eV. In general, however, for both pulse durations recollision excitation to the $n = 1\ 2p\sigma_u$ state [Figs. 5(a) and 5(b)] tends to show poor agreement with experiment. Most notably, though, the biggest drawback of the electron recollision excitation explanation is that it provides no account of the low-KER experimental peak below 3 eV at 7 or 35 fs. None of the calculations we have carried out show any significant dissociation probability on the $D(nl)$ manifolds at low KER. Hence, even if one accepts that electron recollision excitation may play some role, one must still invoke another mechanism to account for the low KER experimental features. Thus, we return our attention to the FTI mechanism suggested by Manschwetus *et al.* [21] as a more plausible explanation that is consistent with all our experimental data, as evident in the following section.

D. Resemblance of FTI to the $D^+ + D^+$ and $D^+ + D(1s)$ channels

As established from the discussion of the FTI classical model of Manschwetus *et al.* [21] (see Sec. III B), the main features of the D^* spectra from FTI should closely resemble those of the D^+ ions produced by the $D^+ + D^+$ and $D^+ + D(1s)$ channels. To check that this is the case, in Figs. 6(a)–6(d) we make a comparison of the D^* [Figs. 6(a) and 6(b)] and D^+ [Figs. 6(c) and 6(d)] spectra. It is noted that the number of D^* counts is arbitrary relative to the number of D^+ counts and, unfortunately, an absolute measurement could not be made for technical reasons. However, as mentioned in Ref. [21], FTI is expected to account for only a small fraction of the D^+ ions (~5%), thus the D^+ spectra will be dominated by the $D^+ + D^+$ and $D^+ + D(1s)$ channels. The

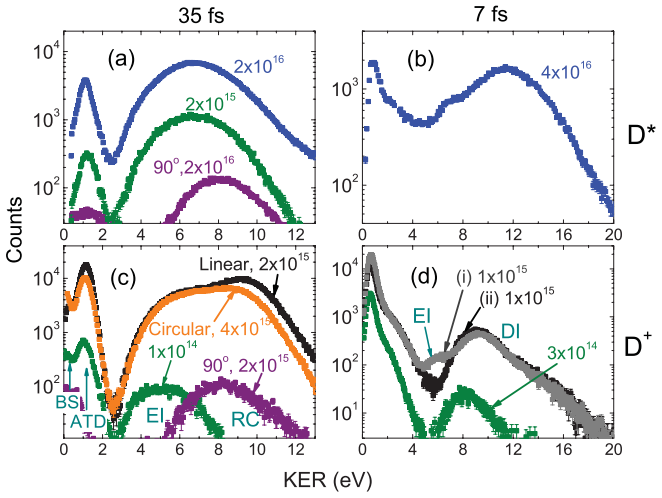

FIG. 6. (Color online) D_2 KER distributions for production of excited D^* atoms in (a) 35 fs and (b) 7 fs pulses. Plots (c) and (d) are the same as (a) and (b) but for production of D^+ ions. The number of D^* counts shown is arbitrary relative to the number of D^+ counts (see text). Intensities are as indicated on the plots in W/cm^2. Most plots are for linear polarization at 0° except for those labeled otherwise. Error bars denote the statistical uncertainty. Note that, in panel (d), measurement (ii) at 10^{15} W/cm^2 is the same as measurement (i) but without the pedestal on the laser pulse.

spectra were recorded using linear polarization with the polarization aligned along the spectrometer axis (0°) unless stated otherwise.

Figure 6(c) shows spectra recorded for D^+ using 35 fs pulses. The individual features of the spectra are well documented in literature [46] and need little introduction. The two low-KER peaks (at 0.3 and 1.2 eV) are from dissociation of D_2^+ to $D^+ + D(1s)$ by bond softening (BS) [47,48] and above-threshold dissociation (ATD) [47–49], respectively. Above 3 eV the peaks are from double ionization of D_2, confirmed by measuring D^+-D^+ coincidences (not shown). The peak at 5.2 eV for 10^{14} W/cm^2 coincides with (charge-resonance) enhanced ionization (EI) [35–37,50]. Increasing the intensity to 2×10^{15} W/cm^2, one ionizes the transient D_2^+ at smaller internuclear distance hence the broadening of the spectra to higher KER. Additionally (inelastic) electron recollision ionization (RC) starts to play a role [13,51], as highlighted by the differences (above 8 eV) with the circular polarization (4×10^{15} W/cm^2), where RC is suppressed. Further evidence of RC is found in the measurement with the laser polarization set to 90° (to the spectrometer axis). EI is suppressed [45] revealing clearly the underlying RC contribution.

For 7 fs pulses [Fig. 6(d)] the D^+ peaks at low KER, like 35 fs, relate to dissociation of D_2^+, except that they extend to higher energy (4 eV), as reported in Ref. [52]. The peaks above 4 eV also arise from double ionization of D_2 but their origin differs from 35 fs. The presence of EI in measurement (i) at 10^{15} W/cm^2 comes from a long pedestal on the few-cycle laser pulses and can be eliminated by careful tuning of the hollow-core fiber, as seen in measurement (ii). This was first noted in Ref. [53]. More notably, the dominant high-KER contribution at 7 fs is from direct ionization (DI). This occurs when the D_2^+ molecule has insufficient time to stretch to the region of EI and is instead ionized directly to the Coulombic state at small R. Measurements using circular polarization show no differences to linear polarization suggesting no RC contribution for 7 fs at the intensities studied (the circular data overlay the linear data and are omitted from the figure for clarity).

We leave it to the reader to carefully inspect the individual features of the D^* spectra in Figs. 6(a) and 6(b) in relation to those of D^+. We simply summarize by stating that overall the features compare remarkably favorably (despite the D^+ spectra being recorded at considerably lower intensities than D^* to avoid detector saturation and space-charge buildup). This strong likeness of the D^* and D^+ spectra lends support to the FTI explanation. One point of particular interest is the fact that the RC peak in the D^+ spectra at 90°, 35 fs appears to be reproduced in the D^* spectra. This is rather fascinating since it suggests that RC plays a double role in the dynamics of D_2: the first electron ionized inelastically scatters off D_2^+ causing secondary ionization, and then at a later stage one of these electrons is captured back to form the excited D^* atoms. Furthermore, evidence of this double-RC event is presented in the ellipticity study in the Appendix.

IV. SUMMARY

In summary, we have presented a detailed synopsis of the recently reported mechanism of electron recapture during D_2 fragmentation. In Ref. [21], Manschwetus *et al.* presented the first evidence for the production of excited Rydberg H^* atoms during strong-field fragmentation of H_2. They explained part of their data in terms of an FTI mechanism [20] whereby one of the Coulomb-exploding H^+ fragments recaptured an ionized electron that had not gained sufficient drift momentum from the laser field to escape the molecule. They also implied that the other part of their data could be explained in a similar way, stemming from bond-softening dissociation of H_2^+.

In line with the work of Manschwetus *et al.*, we have carried out similar measurements of D^* from D_2. By exploring the pulse duration, intensity, fragment angular distribution, and ellipticity dependence of the D^* production mechanism (see Appendix), all evidence that we have indicates that the explanation in Ref. [21] is consistent with our data. We find that the features of the D^* spectra have a direct link with those of our measured D^+ spectra, as anticipated qualitatively from the vision of the FTI mechanism. We also considered the possibility that the experimental data could alternatively be explained in terms of an electron recollision excitation mechanism. Our quantum mechanical calculations appear to show that electron recollision excitation cannot be completely ruled out, but it would seem less satisfactory as an explanation for D^* formation than FTI.

ACKNOWLEDGMENTS

The authors wish to thank Prof. Z. Chang and his group members for assistance with the laser beam. This work was supported by the Chemical Sciences, Geosciences, and Biosciences Division, Office of Basic Energy Sciences, Office of Science, US Department of Energy.

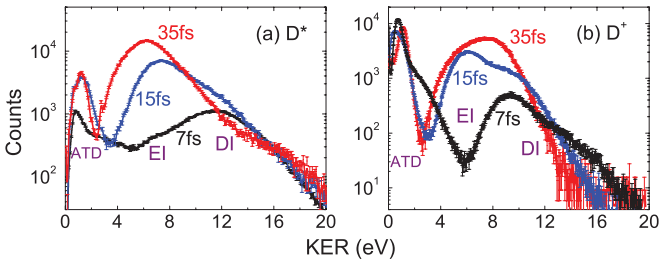

FIG. 7. (Color online) D_2 KER distributions with 7, 15, and 35 fs pulses for the production of (a) excited D^* atoms at 2×10^{16} W/cm^2 and (b) D^+ ions at 10^{15} W/cm^2. Error bars denote the statistical uncertainty.

APPENDIX

For the interest of the reader we present in this Appendix a sequence of measurements that look at the variation of the FTI KER spectra as a function of some of the important laser parameters. Together they comprise a comprehensive picture of FTI.

Dependence on pulse duration. Figure 7(a) shows a plot of the D^* signal for 7, 15, and 35 fs pulses. The spectra are normalized to the same total number of laser shots and are recorded at the same intensity of 2×10^{16} W/cm^2. With decreasing pulse duration the total yield decreases. The probable cause of this is a reduction in double ionization to $D_2{}^{2+}$ for shorter pulses as the transient $D_2{}^+$ is afforded less time to stretch to the region of EI—in accordance with the D^+ spectra shown in Fig. 7(b). The variation with the laser pulse duration reaffirms the structural changes observed in Fig. 6. That is, for shorter (7 fs) pulses, DI at high KER dominates while, for longer (35 fs) pulses, EI dominates.

Intensity. Figures 8(a) and 8(b) display the intensity dependence of the D^* KER distributions for 35 and 7 fs pulses, respectively. Essentially, the signal falls quite rapidly with intensity decrease. One point worth noting is that, at 7 fs, the contribution assigned to EI falls faster than that assigned to DI. This is consistent with earlier studies of H^+ from H_2 [54] lending further credence to the assignment of peaks.

D^* angular distribution. We have measured the angular distribution of the D^* fragments by rotating the laser polarization with respect to the time-of-flight axis of our apparatus from parallel (0°) through to perpendicular (90°). The angular acceptance of the limiting aperture in our apparatus (see Fig. 1) is ±0.9° for D^*; thus, in effect we only collect fragments from molecules that are initially aligned to the TOF axis (assuming of course that there is only weak or no dynamic alignment). Spectra are shown in Figs. 9(a) and 9(b) for 35 fs (2×10^{16} W/cm^2) and 7 fs (4×10^{16} W/cm^2) pulses, respectively.

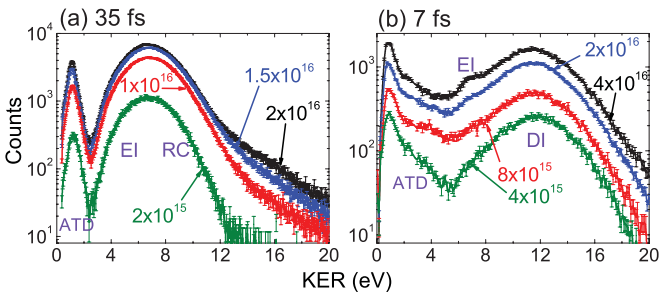

FIG. 8. (Color online) D_2 KER distributions for production of excited D^* atoms as a function of intensity using linearly polarized (a) 35 fs and (b) 7 fs pulses. Intensities (in W/cm^2) are marked on the plots. Error bars denote the statistical uncertainty.

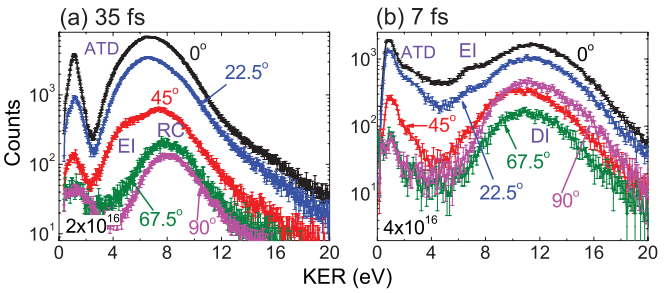

FIG. 9. (Color online) Same as Fig. 8 but showing the dependence on angular distribution of D^* fragments for fixed intensities of (a) 35 fs, 2×10^{16} W/cm^2 and (b) 7 fs, 4×10^{16} W/cm^2. Angles of the laser polarization with respect to the TOF axis are marked on the plots.

Overall, the spectra indicate that D^* formation is most efficient when the laser polarization is along the molecular axis. This concurs with $D_2{}^+$ dissociation and ionization having a similar dependence [55]. At 35 fs, the measurement at 45° appears to reveal a double-hump structure above 3 eV arising from the broad EI and RC contributions centered near 5 and 8 eV, respectively, that merge forming only a single visible peak at 0°. Indeed, at 90° it would seem that EI is highly suppressed with RC being the dominant contribution at this angle. At 7 fs, surprisingly, there is a sizable increase between 67.5° and 90° in the signal arising from DI. We speculate that this may be an indication of competition between the initial DI step that strongly favors alignment and the electron recapture step that may indeed favor perpendicular alignment. From a geometry argument, a drift electron that is ionized along the molecular axis will predominantly experience only the Coulomb field of one of the D^+ ions, while a drift electron ionized perpendicular to the molecular axis can experience the Coulomb field of either of the D^+ ions. However, further investigation is required to determine if this is the correct explanation.

Ellipticity. Although touched upon in Sec. III A, here we briefly review the D^* dependence on the laser ellipticity ϵ. The laser ellipticity dictates whether the ionized electron(s) revisits the parent ion and stays in its vicinity (linear polarization,

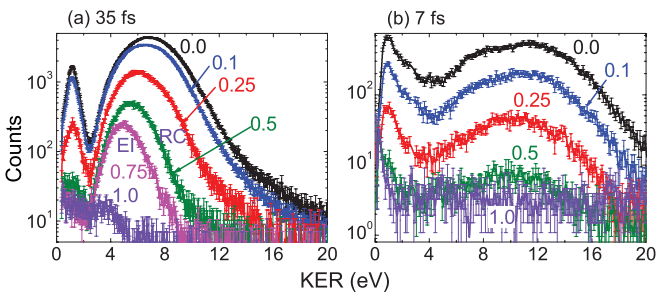

FIG. 10. (Color online) Same as Fig. 8 but showing the dependence on laser ellipticity for fixed peak electric field values matching linearly polarized intensities of (a) 35 fs, 10^{16} W/cm^2 and (b) 7 fs, 2×10^{16} W/cm^2. Ellipticity values (ϵ) are marked on the plots.

$\epsilon = 0.0$) or is driven far from the parent ion with a lateral drift momentum (circular polarization, $\epsilon = 1.0$) [1]. Thus, for linear polarization it is expected that the electron can be recaptured and produce a D^*, while for circular polarization this yield will diminish.

Figures 10(a) and 10(b) show the relevant ellipticity plots for 35 and 7 fs pulses, respectively. In each spectrum the laser intensity is normalized so that the peak E-field amplitude is the same for all ellipticities. The spectra are recorded for a linear intensity of 10^{16} W/cm^2 for 35 fs and 2×10^{16} W/cm^2 for 7 fs.

The expected decrease of D^* signal with increasing ellipticity is observed at each pulse duration. In fact, for circular polarization the D^* yield is almost negligible. Moreover, for 35 fs the high-KER contribution that we suspect comes from electron recollision ionization (RC) of $D_2{}^+$ shows a faster decrease with ellipticity than the rest of the spectrum. This agrees with our suggestion in Sec. III D that electron recollision is involved in two ways in this process: first to inelastically ionize the $D_2{}^+$ and then for one of the electrons to be recaptured back by a D^+ ion to produce excited D^* atoms.

[1] P. B. Corkum, Phys. Rev. Lett. **71**, 1994 (1993).
[2] K. C. Kulander, K. J. Schafer, and J. L. Krause, *Super-Intense Laser-Atom Physics* (Plenum, New York, 1993).
[3] K. J. Schafer, B. Yang, L. F. DiMauro, and K. C. Kulander, Phys. Rev. Lett. **70**, 1599 (1993).
[4] G. G. Paulus, W. Nicklich, H. Xu, P. Lambropoulos, and H. Walther, Phys. Rev. Lett. **72**, 2851 (1994).
[5] D. Ray *et al.*, Phys. Rev. Lett. **100**, 143002 (2008).
[6] M. Okunishi, T. Morishita, G. Prümper, K. Shimada, C. D. Lin, S. Watanabe, and K. Ueda, Phys. Rev. Lett. **100**, 143001 (2008).
[7] M. Meckel *et al.*, Science **320**, 1478 (2008).
[8] M. Peters, T. T. Nguyen-Dang, C. Cornaggia, S. Saugout, E. Charron, A. Keller, and O. Atabek, Phys. Rev. A **83**, 051403(R) (2011).
[9] A. Rudenko, K. Zrost, B. Feuerstein, V. L. B. de Jesus, C. D. Schröter, R. Moshammer, and J. Ullrich, Phys. Rev. Lett. **93**, 253001 (2004).
[10] B. Feuerstein *et al.*, Phys. Rev. Lett. **87**, 043003 (2001).
[11] H. Niikura, F. Légaré, R. Hasbani, A. D. Bandrauk, M. Y. Ivanov, D. M. Villeneuve, and P. B. Corkum, Nature (London) **417**, 917 (2002).
[12] H. Niikura, F. Légaré, R. Hasbani, M. Y. Ivanov, D. M. Villeneuve, and P. B. Corkum, Nature (London) **421**, 826 (2003).
[13] A. S. Alnaser, T. Osipov, E. P. Benis, A. Wech, B. Shan, C. L. Cocke, X. M. Tong, and C. D. Lin, Phys. Rev. Lett. **91**, 163002 (2003).
[14] X. M. Tong, Z. X. Zhao, and C. D. Lin, Phys. Rev. Lett. **91**, 233203 (2003).
[15] A. Paul, R. A. Bartels, R. Tobey, H. Green, S. Weiman, I. P. Christov, M. M. Murnane, H. C. Kapteyn, and S. Backus, Nature (London) **421**, 51 (2003).
[16] I. D. Williams *et al.*, Phys. Rev. Lett. **99**, 173002 (2007).
[17] P. B. Corkum and F. Krausz, Nature Phys. **3**, 381 (2007).
[18] P. B. Corkum and Z. Chang, Opt. Photonics News **19**, 24 (2008).
[19] F. Krausz and M. Ivanov, Rev. Mod. Phys. **81**, 163 (2009).
[20] T. Nubbemeyer, K. Gorling, A. Saenz, U. Eichmann, and W. Sandner, Phys. Rev. Lett. **101**, 233001 (2008).
[21] B. Manschwetus, T. Nubbemeyer, K. Gorling, G. Steinmeyer, U. Eichmann, H. Rottke, and W. Sandner, Phys. Rev. Lett. **102**, 113002 (2009).
[22] T. Nubbemeyer, U. Eichmann, and W. Sandner, J. Phys. B **42**, 134010 (2009).
[23] B. Ulrich, A. Vredenborg, A. Malakzadeh, M. Meckel, K. Cole, M. Smolarski, Z. Chang, T. Jahnke, and R. Dörner, Phys. Rev. A **82**, 013412 (2010).
[24] B. Manschwetus, H. Rottke, G. Steinmeyer, L. Foucar, A. Czasch, H. Schmidt-Böcking, and W. Sandner, Phys. Rev. A **82**, 013413 (2010).
[25] E. Lötstedt, T. Kato, and K. Yamanouchi, Phys. Rev. Lett. **106**, 203001 (2011).
[26] H. Mashiko, C. M. Nakamura, E. M. C. Li, H. Wang, J. Tackett, and Z. Chang, Appl. Phys. Lett. **90**, 161114 (2007).
[27] D. J. Kane and R. Trebino, IEEE J. Quantum Electron. **29**, 571 (1993).
[28] W. C. Wiley and I. H. McLaren, Rev. Sci. Instrum. **26**, 1150 (1955).
[29] P. J. K. Langendam and M. J. Van der Wiel, J. Phys. E **10**, 870 (1977).
[30] A. Robert, O. Sirjean, A. Browaeys, J. Poupard, S. Nowak, D. Boiron, C. I. Westbrook, and A. Aspect, Science **292**, 461 (2001).
[31] F. Penent, P. Lablanquie, R. I. Hall, M. Žitnik, K. Bučar, S. Stranges, R. Richter, M. Alagia, P. Hammond, and J. G. Lambourne, Phys. Rev. Lett. **86**, 2758 (2001).
[32] T. E. Sharp, At. Data Nucl. Data Tables **2**, 119 (1971).
[33] B. D. Esry and H. R. Sadeghpour, Phys. Rev. A **60**, 3604 (1999).
[34] K. N. Shomsky, Z. S. Smith, and S. L. Haan, Phys. Rev. A **79**, 061402 (2009).
[35] T. Zuo and A. D. Bandrauk, Phys. Rev. A **52**, R2511 (1995).
[36] M. Plummer and J. F. McCann, J. Phys. B **29**, 4625 (1996).
[37] L.-Y. Peng, D. Dundas, J. F. McCann, K. T. Taylor, and I. D. Williams, J. Phys. B **36**, L295 (2003).
[38] N. B. Delone and V. P. Krainov, J. Opt. Soc. Am. B **8**, 1207 (1991).
[39] K. C. Kulander, F. H. Mies, and K. J. Schafer, Phys. Rev. A **53**, 2562 (1996).
[40] I. Ben-Itzhak, S. G. Ginther, V. Krishnamurthi, and K. D. Carnes, Phys. Rev. A **51**, 391 (1995).
[41] R. L. Watson, G. Sampoll, V. Horvat, and O. Heber, Phys. Rev. A **53**, 1187 (1996).
[42] J. J. Hua and B. D. Esry, Phys. Rev. A **78**, 055403 (2008).
[43] J. J. Hua and B. D. Esry, J. Phys. B **42**, 085601 (2009).
[44] X. Urbain, B. Fabre, E. M. Staicu-Casagrande, N. de Ruette, V. M. Andrianarijaona, J. Jureta, J. H. Posthumus, A. Saenz, E. Baldit, and C. Cornaggia, Phys. Rev. Lett. **92**, 163004 (2004).

[45] T. K. Kjeldsen and L. B. Madsen, Phys. Rev. Lett. **95**, 073004 (2005).
[46] J. H. Posthumus, Rep. Prog. Phys. **67**, 623 (2004).
[47] P. H. Bucksbaum, A. Zavriyev, H. G. Muller, and D. W. Schumacher, Phys. Rev. Lett. **64**, 1883 (1990).
[48] A. Giusti-Suzor, X. He, O. Atabek, and F. H. Mies, Phys. Rev. Lett. **64**, 515 (1990).
[49] G. Jolicard and O. Atabek, Phys. Rev. A **46**, 5845 (1992).
[50] B. D. Esry, A. M. Sayler, P. Q. Wang, K. D. Carnes, and I. Ben-Itzhak, Phys. Rev. Lett. **97**, 013003 (2006).
[51] A. Staudte *et al*., Phys. Rev. Lett. **98**, 073003 (2007).
[52] J. McKenna *et al*., Phys. Rev. Lett. **100**, 133001 (2008).
[53] A. Rudenko, B. Feuerstein, K. Zrost, V. L. B. de Jesus, T. Ergler, C. Dimopoulou, C. D. Schröter, R. Moshammer, and J. Ullrich, J. Phys. B **38**, 487 (2005).
[54] J. McKenna, B. Srigengan, I. D. Williams, J. Wood, E. M. L. English, W. A. Bryan, W. R. Newell, and I. C. E. Turcu, Central Laser Facility Annual Report, 2004–2005, p. 53, [http://www.clf.rl.ac.uk/Publications/Annual+Reports/2004-05/18222.aspx].
[55] I. Ben-Itzhak, P. Q. Wang, J. F. Xia, A. M. Sayler, M. A. Smith, K. D. Carnes, and B. D. Esry, Phys. Rev. Lett. **95**, 073002 (2005).